Impact Force Profile and Failure Classification of Reinforced Concrete Bridge Columns against Vehicle Impact

Tin V. Do[1], Thong M. Pham[2], and Hong Hao[3]

Abstract

Numerical simulations are utilized in this study to define the impact force profile generated by vehicle collisions on reinforced concrete bridge columns (RCBCs) and classify the dynamic responses and failure of the columns under collision events. The results indicate that both the column properties (i.e. dimension of the cross-section and concrete strength) and initial conditions of vehicles (i.e. vehicle velocity, engine mass, and vehicle mass) play a crucial role in determining the impact force profile from the vehicle collision. A new vehicle impact force model is proposed for engineers to use in design of RCBCs under vehicle collisions in which the influence of shear failure of the column on impact force is considered. Based on the shear mechanism of RCBCs under impact events, the maximum dynamic shear capacity of a column is defined. Furthermore, the bending moment and shear force distributions, as well as the failure mode of RCBCs have been classified into two categories, i.e. flexural response and shear response governed failure with respect to the peak impact force (PIF) on the column. For the flexural response governed failure mode, flexural cracks at the intermediate sections are formed in the positive side of the column, while the diagonal shear or punching shear failure at the

[1]PhD Candidate, Center for Infrastructural Monitoring and Protection, School of Civil and Mechanical Engineering, Curtin University, Kent Street, Bentley, WA 6102, Australia. Email: tin.v.do@postgrad.curtin.edu.au
[2] Research Fellow, Center for Infrastructural Monitoring and Protection, School of Civil and Mechanical Engineering, Curtin University, Kent Street, Bentley, WA 6102, Australia, (corresponding author). Email: thong.pham@curtin.edu.au
[3]John Curtin Distinguished Professor, Center for Infrastructural Monitoring and Protection, School of Civil and Mechanical Engineering, Curtin University, Kent Street, Bentley, WA 6102, Australia, (corresponding author). Email: hong.hao@curtin.edu.au

impact area together with negative flexural-shear cracks occur in the column if the shear failure mode dominant the column responses.

Keywords: Bridge columns; Vehicle collisions; Traffic accidents; Shear mechanism; Failure modes; Impact response; Dynamic effects.

1. Introduction

Vehicle collisions on reinforced concrete bridge columns (RCBCs) from accidents or terrorist attacks occasionally occur. For better protection of bridge structures against vehicle impact a higher demand for the load-carrying capacity of the bridge columns is required. A collision from a heavy-duty vehicle may cause collapse of the whole bridge structure and cost human lives, such as in Texas, 2002 [1] or in Hunan, 2009 [2]. Moreover, a terrorist attack on a bridge column could paralyze the whole traffic system in urban vicinity areas. These accidents and attacks require more attention and understanding for better designs of RCBCs to resist vehicle impacts. Researchers previously tackled this problem through either experimental tests [3], numerical simulations [4-8], or reduced modelling and analyses [9, 10] to study the structural behaviours under impact loads. Among these approaches, the last two methods are more and more widely utilized as compared to the former because of not only high cost and safety concerns associated with the experimental tests but also the ability of achieving high accuracy in predicting the dynamic responses of structures with advanced numerical and analytical models.

Previous researches gave suggestions and recommendations for design of structures to resist vehicle collisions [5, 6, 9, 11-16]. Current design codes and standards commonly adopt a simplified equivalent static force (ESF) to define the impact force from vehicle collision on structures. This approach is straightforward for engineers to estimate the collision force for design analysis of structures. For example, based on the experimental tests on the rigid steel column [3] and the open literature, AASHTO [11] recommended a constant value of about 2,700 kN irrespective of the vehicle loading conditions for design of RCBC to resist vehicle impact. SA/SNZ [12] and CEN [13] suggested a simple equation to calculate the horizontal impact force in which the initial kinetic energy of the vehicle, vehicle deformation, and column displacement are taken into account. CEN [14] distinguished between soft impact, in which the impacted structure absorbs a large amount of energy, and hard impact where the impact energy mostly dissipated by the vehicle, in estimating the equivalent impact force. The maximum impact force on structures is determined based on the elastic behavior of both the vehicle model and structures. However, the deficiencies of the current design guides in predicting the impact force and structural responses are recognized by previous studies [5, 6, 15]. A series of numerical simulations of RCBC subjected to vehicle impacts have been conducted by Abdelkarim and ElGawady [5] to estimate the impact force on structures from collision events. Based on numerical simulation results, an equation to estimate the impact force from vehicle impact on RCBCs based on the kinetic energy of the vehicle model has been proposed. Full-scale models of medium and light truck models have also been used to investigate the impact force and response of steel bollards [10] and concrete-filled steel tubular bollards [17] under vehicle collisions. From these studies, some simplified models to estimate the maximum vehicle impact force on steel structures and barriers have been proposed [10, 17]. However, those studies mainly concentrated on predicting the peak impact force (PIF) on the structure while the impact force profile and duration, as well as the dynamic response of the structures and the parameters affecting the dynamic structural responses, i.e. strain rate effect, vibration characteristics, and inertia force effect are not considered. It is worth mentioning, as will also be demonstrated in this paper, that the peak impact force causes local damage including punching shear or diagonal shear while the global response of the column which may induce different failure modes at other critical sections, such as column top and intermediate sections as systematically presented in the previous study by Do et al. [6], is more correlated to the impact force impulse. Because the current design practice depends mainly on the equivalent static analysis, the reliability and applicability of those proposed models and recommendations based on PIF only are questionable. By presenting the dynamic bending moment, shear force, and acceleration of a RCBC during collision events, Do et al. [6] indicated that the use of the ESF is un-conservative in estimating the impact behavior of the RCBC since the dynamic bending moment and shear force of the column might cause damage which could not be predicted by an equivalent static analysis. An equation to predict the PIF was then proposed in which the mass of the truck's engine is used instead of the total mass of the truck model. The study also provided clear explanations of various observed failure modes of RCBCs in real vehicle accidents. Nevertheless, the latter study was based on a particular column, the influences of the column parameters, such as column height, cross-section dimension, axial force ratio, and steel reinforcements on the impact force profile and the dynamic capacity of the column were not considered in the study. Chen et al. [9] conducted extensive parametric studies on the medium truck collisions on circular and rectangular bridge piers. By separating the impact of the vehicle engine and cargo, the vehicle model was simplified to an equivalent two-degree of freedom model. A coupled mass-spring-damper (CMSD) was developed and validated against numerical results. This study also considered the effects of pier parameters on the time histories of the impact force. However, the elastic material model was used for concrete in the study and the design of the column was almost rigid. Thus, the column could not yield large deformation and displacement by the first peak force caused by engine impact. Importantly, no concrete damage and column failure were considered in the study. Therefore, the numerical results do not necessarily reflect the actual impact behaviour of bridge piers.

The present study aims to propose an impact force profile that would be induced by a vehicle impacting on RCBCs. The effects of column properties e.g. column height, cross-section dimension, axial force ratio, and steel reinforcements under different loading conditions are also considered. Furthermore, based on the shear mechanism of the RCBC under impact load, the maximum achievable impact force from the vehicle collision acting on the column is determined. The responses and failures of the RCBCs are then classified into two categories, i.e. flexural response and shear response, which provide a valuable guidance for engineers in predicting the impact behaviours of the RCBCs.

2. Numerical model development and its verification

2.1. Experimental test and model description

In this study, a three dimensional (3D) finite element (FE) model of a bridge column is developed and verified based on the experimental impact test on a quarter scaled reinforced concrete (RC) column by Zhang et al. [18]. The schematic view, column design, and the pendulum impact test setup are shown in Fig. 1a. To simulate the impact response of the tested column in the numerical model, the concrete column, steel impactor, footing and the added weight are modelled by hexahedral elements with 1 integration point while the longitudinal and transverse reinforcements are modelled by 3-nodes beam elements with 2 x 2 Gauss quadrature integration. In the simulation, the contact between the reinforcement bars and the surrounding concrete is assumed as a perfectly bonded since no slippage between the reinforcements and concrete was observed in the experiments. In addition, the LS-DYNA contact algorithm named *Contact_Automatic_Surface_to_Surface (ASTS) is utilized to model the impacting contact between the steel impactor and the RC column. Since no displacements or rotation at the connection between the footing and the floor was observed during the test [18], the column is fixed at the bottom face of the footing in the FE model. The numerical model of the pendulum impact test on the RC column is shown in Fig. 1b.

2.2. Material models and strain rate effects

The LS-DYNA software provides several types of material models which can be used to simulate the concrete behaviors subjected to impact and blast loads, e.g. Mat_Winfrith_Concrete (Mat_084_085), Mat_Concrete_Damage (Mat_072), Mat_CSCM_Concrete (Mat_159), and Mat_Concrete_Damage_Rel3 (Mat_072R3) [19]. In this simulation, the Mat_072R3 is employed where the plasticity, shear damage, and strain rate effects of the concrete are under consideration. Only the unconfined compressive strength of concrete, i.e., 34 MPa in this study, is required as input for this material model while other parameters of concrete material properties can be automatically created [19]. This model is most commonly used to simulate concrete material behaviours under blast and impact loads, its reliability has been intensively verified [20-23]. The compressive and tensile dynamic increase factor (DIF) of the concrete material proposed by Hao and Hao [24] are utilized in this study to model the dynamic increase in concrete material strength. Furthermore, the LS-DYNA function named Mat_Add_Erosion is also employed to remove the damaged elements of concrete during the impact process to avoid computation over-flow. This study uses the maximum principal strain at failure as a criterion to delete the failed concrete elements. The value of 0.7 is utilized as the erosion criterion for the concrete of the two columns after trials, which yield a good prediction of the column damage. It should be noted that the erosion algorithm is trial and error based because it has no solid physical background and violates energy and momentum conservation.

In addition, Mat_Piecewise_Linear_Plasticity (Mat_24) is used to model the longitudinal and transverse reinforcements. The Young's modulus, mass density, and Poisson's ratio of the steel reinforcement are 200 GPa, 7800 kg/m^3, and 0.3, respectively. The yield strength of the transverse reinforcements is 300 MPa while that of the longitudinal reinforcement is 500 MPa. The DIF of these reinforcements which was proposed by Malvar and Crawford [25] is used. Besides, Mat_Elastic (Mat_001) is chosen for modeling the solid steel impactor with the Young's modulus, mass density, and Poisson's ratio of 200 GPa, 7800 kg/m^3, and 0.3, respectively.

2.3. Model verification and comparisons

The numerical results are verified against the experimental results in which the impact force time histories, lateral displacement, and column plastic strain versus failure of the column are compared in Fig. 2. As shown in Fig. 2a, the crack patterns of the concrete column including flexural cracks at the column mid-height and the diagonal shear crack at the column base which were observed in the experimental test are well simulated by the FE model. Moreover, the PIF, impact duration, and the global trend of the impact force time histories from the numerical model also well agree with the testing data as shown in Fig. 2b. Furthermore, the simulation shows a good prediction of the lateral displacement time histories at the column mid-height in which the maximum and residual displacements in the experimental test were 7.5 mm and 1.5 mm, respectively, compared to 7.8 mm and 1.8 mm in the FE model, respectively (see Fig. 2c).

2.4. Verification of full-scale bridge column under vehicle collisions

From the above comparisons, the numerical simulation has ability to simulate the impact force, lateral displacement, and failure modes of the scaled RC column under low impact velocity of the lab test. However, concerns about the responses of a large-scaled RC column under high impact velocity of collision accidents still remain. Thus, in this section, a full-scale bridge column under real vehicle accident on IH-30 near Mount Pleasant, Texas [1] is employed and simulated to verify the accuracy of the current simulation. In this accidental collision, the bridge column which had a circular cross-section of 762 mm was impacted by a heavy-truck-trailer with the total mass of 30 ton. The column was designed with eight-30-mm-diameter longitudinal bars and 10-mm-diameter transverse bars at 150 mm spacing [1]. By using the above material model, strain rate effects, and modelling techniques, a 3D FE model of the mentioned column is built and impacted by the heavy-truck-trailer model as presented in Fig. 3a. It should be mentioned that the vehicle model was adopted in the previous study and shared by Sharma et al. [4]. The truck information will be presented in Section 3. Because no impact force and displacement of the column were reported from the collision, the failure mode of the column in the simulation is used to compare with the real accident as presented in Fig. 3b. The figure shows that the failure of the column i.e. diagonal shear at the base, flexural – shear failure at the column mid-height, and flexural crack at the column top from the real vehicle collision are well simulated in the numerical model. These verifications show the reliability and accuracy of the current simulation techniques in predicting the impact responses of the RC structures with different sizes under wide ranges of velocities.

3. Simulation of bridge specimens and vehicle models

The numerical model of a full-scale RC bridge is developed in this section based on the previously validated material models, strain rate effects, contact definitions, and modeling techniques. The RC bridge consists of one single RCBC, two hollow-section girders as superstructures and two concrete abutments, as shown in Fig. 4. Similar bridge model was also employed in previous studies to investigate the pier responses [15, 26] and the accuracy of this modeling approach in simulating and predicting the dynamic response of RC columns under impact loading has been confirmed [27]. The reference RCBC (C0) used in this study is 1,200 mm x 1,200 mm (*D* x *W*) in cross-section and 9,600 mm in height (*H*) while the overall dimensions of the hollow beam are obtained from Megally et al. [28] with the span length of 40 m. The weight of the superstructure which equals 10% of the vertical compressive capacity of the column is transmitted to the RC column through a cap beam placed on the column top (see Fig. 4). The coefficient of friction between the superstructure and the cap beam or the concrete abutment is assumed to be 0.6 [6, 29]. No bearing pad or rubber is included in the model due to its insignificant effect on the behaviors of the column under vehicle impact [15]. The column is reinforced with twenty-four 30-mm-diameter longitudinal rebars extending from the footing to the cap beam and 14-mm-diameter transverse bars at 200 mm spacing. In the numerical simulation, the footing, RCBC, cap beam, superstructure, and abutments are simulated by hexahedral elements with one integration point (constant stress solid elements) while the steel reinforcements were modelled by 3 nodes-beam elements. The convergence test is conducted to determine the optimal mesh size of the concrete and steel element based on a balance between simulation accuracy and computational efficiency. The numerical results converge when the mesh size of concrete is 20 mm. Since the response of the column during the impact force phase is the primary concern in this study, the implicit simulation is terminated at about 300 - 500 ms (a half of natural period of the column). Therefore, the system damping is ignored in the present study.

The heavy truck trailer as mentioned previously (see Fig. 3) and a medium Ford truck model (see Fig. 4a) are used to represent the truck impact on the RCBC in this study. The medium truck model has been commonly used to analyze the impact behaviors of structures under vehicle collision [4-6, 9, 15, 26, 30, 31]. The Ford truck model was modeled and validated by FHWA/NHTSA National Crash Analysis Centre at the George Washington University. The total mass and engine mass of the Ford truck model are 8 ton and 0.64 ton, respectively. In this study, the vehicle model is assumed to impact at 1.5 m above the top face of the footing as shown in Fig. 3a. Without loss of generality, three loading cases of the medium truck are firstly considered in this study including (1) Load 1: the vehicle velocity of 100 km/h with the engine mass of 0.64 ton, (2) Load 2: the vehicle velocity of 100 km/h with the engine mass of 2.0 ton, and (3) Load 3: the vehicle velocity of 120 km/h with the engine mass of 2.0 ton. These loading conditions are chosen since they cause three different failure modes of the columns consisting of flexural cracks, local diagonal shear failure, and punching shear failure at the impact area [6]. It should be noted that the numerical results from different vehicle velocities from 60 km/h to 140 km/h in the previous study [6] are utilized in this study to propose the impact force profile. The total mass of the medium truck ranging from 2.7 ton to 11.8 ton is used in these simulations as suggested by Sharma et al. [4]. The proposed impact force profile is applicable for both the medium truck and the heavy truck. The total mass and the engine mass of the heavy truck trailer are 12 ton and 1.5 ton, respectively. To investigate the impact force profile of the heavy truck collision under wide ranges of vehicle mass and velocity, the total mass of the heavy truck trailer varies from 17 ton to 37 ton while the vehicle velocity increases from 80 km/h to 110 km/h. It is worth mentioning that the light truck with the total mass smaller than 2.7 ton [4] is not considered in this study because of its less significance on the column response [5, 15]. In this study, the contact algorithm named the penalty method via the ASTS contact keywords is used to define the contact between the vehicle model and the RCBC. Four main parameters need to be defined in this contact algorithm including the penalty formulation (*SOFT*), the penalty scale factor (*SLSFAC*), and the scale factor for slave stiffness (*SFS*) and master stiffness (*SFM*). In the simulations, the standard penalty formulation (*SOFT* = 0) is employed while the default value of penalty scale factor (*SLSFAC*) at 0.1 is adopted. Moreover, the default value of *SFS/SFM* at 1.0/1.0 is used. The corresponding parameters in this study are adopted from the previous study [21].

In the following sections, the RCBCs with different column heights, cross-section dimension, transverse reinforcements, axial load ratio, and longitudinal reinforcements under three different loading conditions are examined. These column parameters are chosen because of their significant contribution to the column global stiffness, shear capacity, and flexural capacity of the column which govern the impact performances, crack patterns, and damage of the RCBC. Firstly, the column cross-section is kept constant at 1,200 mm x 1,200 mm while five different column heights, i.e. 4,800 mm, 6,000 mm, 7,200 mm, 9,600 mm, and 12,000 mm are considered to investigate the influences of the slenderness ratio (*H/D* = 4, 5, 6, 8, and 10) of the column on the impact force and failure modes of the column. Moreover, five cross-section dimensions with D x W (depth x width) = 600 mm x 600 mm, 800 mm x 800 mm, 1,200 mm x 1,200 mm, 1,500 mm x 1,500 mm, and 2,000 mm x 2,000 mm are considered while the slenderness ratio of these columns is kept at 8. Furthermore, three different transverse reinforcement ratios, i.e. 0.09% (d8s200), 0.26% (d14s200), and 0.53% (d14s100) are used to examine the effects of the transverse reinforcements in controlling the response of the column. The bending moment capacity of the column influenced by the initial axial load and the longitudinal reinforcement ratios is also taken into consideration. The initial axial force applied on the column is increased from 10% to 20%, 40%, and 60% of the column axial compressive capacity while the longitudinal reinforcements vary from 0.63% (24d22) to 1.16% (24d30) and 1.70% (24d36), respectively. Table 1 summarizes the considered column configurations and the corresponding numerical results.

4. Vehicle impact force profile model

4.1. Medium truck model (mass < 12 ton)

The impact force time histories on the RCBC C0 from the first loading condition (Load 1) is presented in Fig. 5. Based on the understanding from the previous studies [9, 16, 31, 32] and the numerical results in this study, the impact force time histories from a truck impact on the RCBC can be idealized in four stages as shown in Fig. 5. Firstly, the truck bumper collides on the RCBC generating the first impact force plateau P_1 with duration t_{P1}. The impact force then increases to the F_1 due to the collision of the vehicle engine with duration t_{F1}. After that, the impact force drops to P_2 and keeps constant due to the impact of the truck rails and vehicle parts placed between the engine and the cargo with duration t_{P2}. Finally, the impact of vehicle cargo causes the second peak, F_2, on the column. The impact of the cargo increases the force from P_2 to F_2 in the period of t_{F2}, and the impact force then decreases to zero at 165 ms. The above impact force and duration corresponding to various vehicle impact scenarios and bridge configurations are determined based on the numerical simulations in this study. It should be noted that the total impact force duration is taken as 165 ms in this study. The value is approximated based on many simulation cases carried out in the study. It is noted, however, the value is valid only for the medium truck model considered in the study. For other vehicle models and other impact scenarios, the total impact duration might be different.

It is well-known that the truck engine colliding on the column occurs only after the bumper totally deformed due to the collision. Thus, the duration of the first stage primarily depends on the gap between the bumper and the vehicle engine. Besides, the impact duration definitely relates to the impact interaction, impact velocity, and the relative stiffness between impactors and structures. By presenting the force-deformation curves of the bumper during the impact event, the previous studies [9, 17] indicated that stiffness of the bumper is marginal compared to that of a bridge pier. Therefore the duration of this phase is normally short compared to the total duration of a collision event (see Fig. 5). From the numerical results, it is found that the velocity of the vehicle slightly reduces from V when impact starts to about $0.9V$ when the engine impacts on the column in which V is the initial vehicle velocity (m/s) upon collision. To represent the velocity during this period, the average velocity of $0.95V$ is assumed. The duration of the bumper impact phase can then be obtained from the gap between the bumper and the engine box, L_{1M} *(mm)*, and the velocity of the truck, V *(m/s)*, expressed as follows:

$$t_{P1} = \frac{L_{1M}}{0.95V}(ms) \qquad (1)$$

Generally, L_{1M} is 660 mm [17], 550 mm [9], and 500 mm [30], depending on the vehicle model. In this study, L_{1M} is taken as 550 mm for the medium-duty truck model collided on the RC column. This number can be easily changed to fit a particular truck in real design.

In each simulation, P_1 can be determined by dividing the total impulse of the bumper's impact to the impact duration t_{P1}, (see Fig. 6a) which is given in Table 1. As can be seen that P_1

significantly depends on the column width and impact velocity of the truck while the influence of the slenderness, initial axial force ratio, and steel reinforcements is marginal and can be negligible. P_1 shows a proportional increase trend with the increase of the column width, as shown in Fig. 6b. This is because the increase in the column width increases the contact area between the bumper and the column, resulting in a higher impact force. Besides, the relationship between the force P_1 and the impact velocity which obtained from [6] is also plotted in Fig. 6c. Based on these numerical results, the force P_1 can be generalized as follows:

$$P_1 = P_0 \times k_1 \times k_2 (kN) \tag{2}$$

$$k_1 = 0.788 \frac{V}{27.78} + 0.240 \tag{3}$$

$$k_2 = 0.559 \frac{W}{1200} + 0.441 \tag{4}$$

where k_1 and k_2 are the dimensionless coefficients describing the effects of the dimension and impact velocity on P_1, respectively (see Fig. 6b and c); W is the column width (mm); $P_0 = 1,683 (kN)$ is the average value obtained from the simulations corresponding to a column width of 1,200 mm and the impact velocity of 100 km/h. The column section of 1,200 mm x 1,200 mm and velocity of 100 km/h are selected since these values are commonly used in the real application.

The truck's engine then impacts on the column through the vehicle bumper which has been deformed due to the truck's frontal impact and currently placed between the engine box and the column. The impact force from the engine causes the deformation of the vehicle bumper which not only dissipates an amount of the impact energy but also affects the contact stiffness between the column and the engine box. The previous study by Pham et al. [21] has indicated that a minor change of the contact stiffness between a structure and an impactor may cause a significant difference in the impact force. Thus, the impulse from the engine impact is complicated and might not be easily predicted from the theory of momentum – impulse conversion. Hence, the F_1 and the impact duration of the engine impact in this study is estimated through the numerical results. The variation of the t_{F1} under different loading conditions are presented in Fig. 7. According to the previous results from Chen et al. [9] and Do et al. [6], the influences of the vehicle speed on the impact duration of the engine impact is also presented in Fig. 7. It is clear that the increase in the impact velocity (from 16.67 m/s to 38.89 m/s) shows a substantial decrease in the impact duration (from 25 ms to 5.5 ms). Fig. 7b shows that t_{F1} is almost unchanged even though the column width increases from 800 mm to 2,000 mm when these columns are under the same loading conditions. Moreover, by comparing Fig. 7a and Fig. 7b, with the same impact speed (27.78 m/s – Load 2) but different engine's mass (0.64 ton compared to 2.0 ton), the duration of the engine impact is also similar (8.5 ms). These results demonstrate the relative independence of the duration t_{F1} on the engine's mass and the column's width but this duration is affected by the impact velocity. From the above observations, t_{F1} can be estimated from the truck velocity by the following equation (see Fig. 7c):

$$t_{F1} = \frac{4,147.4}{V^{1.833}}(ms) \tag{5}$$

F_1 highly depends on the cross-section dimension, impact velocity, and the engine mass while the influence of the other parameters is insignificant, as given in Table 1. Furthermore, the insignificant effect of structure span and concrete strength on the PIF, which is the same as F_1 defined in this study, have been previously reported [32-34]. F_1 on the RCBC with different column cross-sections under three conditions is also plotted in Fig. 8. It can be seen that F_1 from the engine impact increases with the engine mass and vehicle velocity, but cannot be higher than the maximum dynamic shear capacity of the column, $P_{dyn}^{\max}$ (Columns C5 and C6) which will be determined and discussed in the subsequent section. This is because when the impact force from the engine impact reaches the $P_{dyn}^{\max}$, it induces the punching shear cracks on the column, resulting in a slight movement of the shear plug. This relative displacement of the impacted area of the column affects the vehicle - column interaction and reduces the impact force on the column. Moreover, considering the equilibrium condition of vehicle impact, F_1 cannot be larger than the total column resistance because the column would fail if it reaches the column resistance. Based on the above observations, F_1 on the RCBC can be updated from the previous studies [6] by considering the failure of the concrete column as:

$$F_1(kN) = 969.3\sqrt{0.5m_eV^2} - 7{,}345.9 \le P_{dyn}^{\max} \qquad (16.7 \text{ m/s} < V < 40 \text{ m/s}) \qquad (6)$$

where m_e is the mass of the engine (ton); $P_{dyn}^{\max}$ is the maximum dynamic shear capacity of the column.

In the third stage, the impact force drops to P_2 and lasts until the vehicle cargo collides on the column. As presented in Fig. 9a, the cargo gradually moves 1,600 mm before colliding on the frontal parts, e.g. the vehicle cabin and the bumper, and resulting in the second peak on the column (see Fig. 9b). It should be noted that although the distance between the cargo and the cabin is about 480 mm, the cargo collides on the cabin after moving about 1,600 mm because of the densification of the frontal parts of the vehicle. The cargo stops impacting on the column at about 165 ms after shifting about 2,400 mm. As shown in Fig. 9a, those values are independent of the vehicle velocity. A similar observation is also reported in the previous study by Chen et al. [9] when the cargo stops colliding on the structure after moving about 2,500 mm. The displacement time history of the cargo is thus simplified as a bi-linear curve as illustrated in Fig. 9c. In the first part, the cargo displacement increases linearly with time, having a slope coefficient of $0.85V$. The coefficient is 0.85 owing to the reduction of the vehicle velocity due to the collision and the effect of the frame stiffness. It is assumed that when the cargo moves about 2,400 mm, it will cause the second peak, F_2 on the column and the impact force time histories then decreases linearly to zero at 165 ms. Thus, the impact duration t_{P2} and t_{F2} can be determined as follows:

$$t_{P2} = \frac{1,600}{0.85V} - t_{P1} - t_{PIF} = \frac{1,303}{V} - \frac{4,147.4}{V^{1.833}}(ms) \tag{7}$$

$$t_{F2} = \frac{2,400}{0.85V} - \frac{1,600}{0.85V} = \frac{940}{V}(ms) \tag{8}$$

Additionally, P_2 is determined by dividing the total impulse of the third stage to the impact duration t_{P2}. In each simulation, the impulse of the third impact is defined by integrating the impact force time histories from the numerical simulation. As given in Table 1, The P_2 is almost identical in all the simulations. Thus, the influences of the column parameters and the initial conditions of the vehicle model on P_2 is neglected. In this study, the P_2 is taken as 1,290 kN after averaging from all the numerical results. Eventually, the second peak, F_2, from the cargo impact can be defined based on the initial momentum – impulse conversion as adopted in the previous studies [6, 31], as given below:

$$F_2 = \frac{1000mV - \left[P_1\left(t_{P1} + \frac{t_{PIF}}{4}\right) + PIF\frac{t_{PIF}}{2} + P_2\left(\frac{t_{PIF}}{4} + t_{P2} + \frac{t_{F2}}{2}\right)\right]}{\frac{1}{2}\left[165 - (t_{P1} + t_{PIF} + t_{P2})\right]}(kN) \geq 0 \tag{9}$$

where m is the total mass of the vehicle model (ton);

In case the diagonal shear failure or punching shear failure occurs on the RCBC resulting from the F_1, the impact force time histories will last until the impact energy fully transfers to the column without the second peak from the cargo's impact, as presented in Figs. 10b, c, and e. This is because the failure of the column leads to the movement of the column together with the vehicle model in the impacted area resulting in the considerable reduction of the column resistance. It is worth mentioning that previous studies usually neglect vehicle-column interaction and local damage of column in predicting the impact force of the RCBC, which might not lead to accurate predictions as demonstrated above, but overpredict the impact force from cargo. The impact duration of P_2 can be calculated as follows:

$$t_{P2b} = \frac{1000mV - \left[P_1 \left(t_{P1} + \frac{t_{PIF}}{4} \right) + PIF \frac{t_{PIF}}{2} + P_2 \frac{t_{PIF}}{4} \right]}{P_2} (ms) \tag{10}$$

where t_{P2b} (ms) is the duration of the third stage when the column exhibits a shear failure due to F_1.

The comparisons of the proposed impact force profile and the numerical simulation for various loading conditions are presented in Fig. 10. Moreover, to verify the reliability of the proposed model on predicting the impact force time histories of collision events with different vehicle mass, the total mass of the vehicle is increased from 8 ton to 11 ton by increasing the cargo mass from 3 ton to 6 ton while the mass of the engine is 0.64 ton. As presented in Fig. 11, the proposed model also provides a good estimation of the impact force time histories including the impact force peaks, duration, and impulse in the wide range of the vehicle mass. These comparisons and verification indicate that the proposed vehicle impact force profile model for medium truck reliably predicts the impact force of vehicle collisions on bridge piers with various vehicle's mass, engine mass, vehicle velocity, and structural properties. It should be noted that the cargo, which has a higher mass than vehicle engine, impacts on the columns in these examples do not induce a large peak force F_2 because the column has suffered substantial damage due to the engine impact. If the column is very stiff and does not suffer prominent damage due to engine impact, cargo impact would generate a large impact force F_2, as observed in some previous studies that either assumed the column is rigid or linear elastic [9, 35].

4.2. Heavy truck trailer

To verify the accuracy of the proposed impact force profile on different vehicle models and velocities, the heavy trailer model is considered in this section. The vehicle velocity of the heavy trailer considered in the analysis increases from 80 km/h to 110 km/h (H1 – H3) and the total mass ranges from 17 ton to 37 ton (H4 – H5), as given in Table 2. The impact force time histories on the RCBC from the heavy trailer is shown in Fig. 12. Similar to the medium truck model, the impact force time histories of the heavy truck also includes four stages in which the impact of bumper and truck rails create two plateau stages (P1 and P2) while the engine and cargo impact cause two peak impact forces (F1 and F2) during the whole impact process. As mentioned previously, each vehicle model has different length and characteristics leading to a different impact duration and its amplitude. The numerical results of the heavy truck impacted on the RCBC are given in Table 2. From the numerical simulation results and using the same analysis methods as in the previous section, the impact duration of each impact stage from the heavy truck can be summarized as follows:

$$t_{P1} = \frac{L_{1H}}{0.95V}(ms) \tag{11}$$

$$t_{P2} = \frac{800}{0.85V}(ms) \tag{12}$$

$$t_{F2} = 2.1\left(m-12\right)+5.6(ms) \tag{13}$$

where L_{1H} (ms) is taken as 940 mm for the heavy truck model collided on the RC column. It should be noted that as observed from the numerical simulations, the Eqs. (2), (5), and (6) to define P_1, t_{F1}, and F_1, respectively, of the heavy truck are similar to these for the medium truck. Moreover, the second plateau P_2 is suggested as 850 kN for the heavy truck trailer. As previously discussed, if a column survives from the engine impact, it then suffers the impact from the cargo. In this study, the cargo mass of the heavy truck is increased from 5 ton 25 ton in the analyses, the peak impact force from the cargo impact, F_2, is almost similar in these simulations as expected (see Fig. 12b). Even though the columns in these simulations do not fail by the impact of the engine, it causes local damage to concrete at the impact area. As a result, the contact stiffness between the column and the truck model is significantly reduced when the cargo impacts the column. The reduction of the contact stiffness thus reduces the peak value of the cargo impact [21] as compared to the engine impact although the mass of the cargo is considerably larger than that of the engine. However, the impulse of the second peak impact force is greater than the first one, which reflects the huge kinetic energy carried by the cargo. It is worth mentioning that although the peak impact force of the cargo impact is approximately unchanged, the impulse from the cargo impact significantly increases when the mass and the velocity of the cargo increases, as shown in Fig. 12. From the numerical results, the second peak impact force F_2 is taken as 7,000 kN in this study (see Table 2). The total impact duration, t_{total}, from the heavy truck collision to the RCBC thus can be obtained in the following equation:

$$t_{total} = t_{P1} + t_{PIF} + t_{P2} + t_{F2} + t_{F2-R} (ms) \tag{14a}$$

$$t_{F2-R} = \frac{1000mV - \left[P_1\left(t_{P1} + \frac{t_{PIF}}{4} \right) + PIF\frac{t_{PIF}}{2} + P_2\left(\frac{t_{PIF}}{4} + t_{P2} \right) + \left(P_2 + F_2 \right)\frac{t_{F2}}{2} \right]}{\frac{1}{2}F_2} (ms) \tag{14b}$$

where t_{F2-R} (ms) is the duration from the peak impact force, F_2, to zero point.

It is noted that the impact duration, t_{P2}, is estimated by using Eq. (10) in both scenarios: (1) diagonal shear or punching shear failure occurred at the vicinity of the impacted area due to the first peak impact force F_1 and (2) no added mass applied to the heavy truck model. The comparisons between the proposed impact force profile model for the heavy truck and the numerical simulation results are presented in Fig. 13. The comparison shows that the proposed impact force profile, the peak impact forces from the engine and the cargo impact, impact duration of each single impact phase, and the total impact duration can be well predicted.

There is a consensus that the change of vehicle model may slightly change the duration and the magnitude of impact force in each impact stage. Therefore, the use of two vehicle models in the simulation does not imply that these results are applicable for only these two particular vehicle models. The numerical results in this study demonstrate that even the vehicle models are different, the PIF caused by the vehicle engine and the impulse of the collision show a consistent trend. The variations of the column properties do not have a significant influence on the PIF either. It should be highlighted that the PIF and the impulse of the impact are the crucial parameters determining the response of RCBC under vehicle collision [6, 31]. To design bridge columns against vehicle collisions, the input information for estimating impact loads includes vehicle speed, engine mass, total mass of the vehicle, the frontal design of the vehicle, and the gap between the engine mass and cargo mass. With these parameters, the proposed equations can be used to estimate the impact force time histories. The proposed impact force models also fit well with RC columns of rectangular or square sections with different sizes. However, the use of other column cross-section types, e.g. circular section and concrete-filled steel tube, may have a slight influence on the magnitude of the impact force since the contact stiffness between the vehicle model and column is changed. Therefore, studies on the effects of cross-section types on the impact force are required. The accuracy of the proposed method also needs to be carefully validated in future works.

5. Shear mechanism of RC structures

The shear mechanism of the concrete structures under impact loads has been experimentally and numerically investigated in previous studies [33, 36-38]. In these studies, the punching shear failure is the most common failure scenario of the concrete beams under severe impact loading conditions. Likewise, the example rectangular RC columns impacted by a vehicle model showed punching shear failure at the impact area when the PIF reaches 30,000kN, which is larger than the shear capacity of the column section, caused by the engine impact [6] (see Fig. 14a). Based on the shear failure mode of the concrete structures under impact loads, with the crack patterns related to punching shear failure as shown in Fig. 14b, the dynamic shear capacity of the column, $P_{dyn}^{\max}$, can be written as

$$P_{dyn}^{\max} = 2 \times (DIF_c \times V_c + DIF_s \times V_s) + \sum ma \quad (15)$$

$$V_c = f_t \times \cos\alpha \times \frac{W \times D}{\sin\alpha} = f_t \times W \times D \quad (16)$$

where DIF_c and DIF_s are the dynamic increase factors of the concrete and steel material strength in the diagonal section, respectively; V_c and V_s are the contribution of the concrete and the steel reinforcement to resist the shear force, respectively; m and a are the mass and acceleration of the shear plug, respectively; f_t is the tensile strength of the concrete; α is the inclined angle of the diagonal crack ($\alpha = 45^{o}$).

In the previous studies, the contribution of transverse reinforcements and FRP wraps to the shear capacity of the concrete beams have been examined. Four different transverse reinforcement ratios, e.g. 0.0%, 0.1%, 0.2 %, and 0.4% were examined under drop-weight tests by Saatci [37]. The experimental tests showed that the increase of the shear reinforcement reduced the crack width of the concrete beams but all the tested beams experienced shear-plug cracks under the impact load. It is worth mentioning that although the shear strength of the concrete and transverse reinforcements of the tested beam exceeded the impact force, the diagonal shear cracks at two sides of the impact point, forming punching shear was observed for the beam even with the highest transverse reinforcement ratio of 0.4%. A similar observation was also obtained in the previous studies based on numerical simulations [21, 36] where the punching shear failure was formed in the concrete beams under impact loads even though the shear reinforcements were significantly increased. The use of FRP U- wraps improved the shear resistance of concrete beams under impact load by reducing the shear crack width and increasing the stability of the concrete beams as reported by Pham and Hao [38]. However, the punching shear cracks still occurred at the impact point when the impact force reaches its peak. These studies demonstrated that the use of the shear reinforcement or FRP wraps might reduce the crack width and increase the post-impact behaviour of the concrete structures but showed a minor contribution to resisting the punching shear failure of the reinforced concrete beams. To examine the performance of reinforced concrete columns under vehicle impact, the strain time histories of concrete and steel are plotted in Fig. 15 (C0-Load 2). It is clear that when damage to concrete occurs due to the tensile failure at strain of $1.75e^{-4}$ at about 25.5 ms, the strain of transverse reinforcement ($2.23e^{-4}$) is about 9% of its yield strain ($2.5e^{-3}$). It is assumed that the concrete and the steel reinforcement are perfectly bonded. Thus, when the column exhibits the punching shear cracks, the strain of the shear reinforcement equals the failure strain of the concrete, ε^t_c. Hence, the total tensile force, V_s, in the shear reinforcements can be estimated as follows:

$$V_s = E_s \varepsilon^t_c \times 2A_s \times n \tag{17}$$

$$A_s \approx \frac{W \times D \times \delta}{4n} \tag{18}$$

where E_s is the Young's modulus of the steel reinforcements; A_s is the cross-section area of a single shear rebar; n is the number of steel legs in one side of the shear-plug; δ is the shear reinforcement ratio.

From Eq. (16) and Eq. (17), the V_s can be determined by the following equation:

$$V_s = \frac{E_s \varepsilon^t_c}{2f_t} \times \delta \times W \times D \times f_t = \frac{E_s}{E^t_c} \times \frac{\delta}{2} \times V_c \tag{19}$$

Normally, the shear reinforcement ratio, δ, in the previous studies ranged from 0.5% to 1%. Therefore, from Eq. (19) at the peak impact force, the contribution of the shear reinforcement to the total shear capacity of the column is minor compared to the concrete (2.5-5%). This is why the increase of the shear reinforcement from the previous studies showed a minor effect on the shear capacity in preventing the occurrence of the punching shear cracks in concrete structures. It should be highlighted that after the occurrence of punching shear cracks in concrete structures, the contribution of the shear reinforcement is then crucial in controlling the stability of the structures (see Fig. 15b). In brief, the shear reinforcements significantly improve the shear resistance of RC structures but do not help to prevent cracks in concrete from occurring. In dynamic response, once cracks occur, they allow relative movement between the shear plug and the vicinity parts. This slight relative movement has little effect on the shear resistance of the structures under static loads, however, it significantly reduces the inertia resistance since the vehicle and the shear plug can move together. This is the reason why once shear cracks happen in the columns under impact, the peak impact force cannot increase further. The dynamic shear capacity of the RCBC, neglecting the contribution of the shear reinforcements, can be estimated by the following equation:

$$P_{dyn}^{\max} = 2\times DIF_c \times f_t \times D\times W + a\times \rho_c \times \left(D+H_I\right)\times D\times W \tag{20}$$

where H_I is the height of the impact area, as given in Fig. 14b.

It should be mentioned that each concrete and steel element in the shear-plug area has a different DIF and different acceleration. It is very complicated and difficult to determine these values by solving the dynamic equilibrium equation. Adhikary et al. [39] proposed an empirical equation to predict DIF of the maximum capacity of a RC deep beam under impact load based on the shear span ratio, loading rate, longitudinal and shear reinforcement ratio. However, the contribution of the inertia force was neglected in that study due to the loading rate was under 2 (m/s). In this study, the effect of the DIF and inertia force in the shear plug area is simplified by using a dimensionless coefficient, k_T, as follows:

$$P_{dyn}^{\max} = 2\times \left(DIF_c + \frac{a\times \rho_c \times \left(D+H_I\right)}{f_t} \right)\times f_t \times D\times W = k_T \times f_t \times D\times W \tag{21}$$

From the numerical results, the punching shear failure occurs on the column C5 and C6 when the PIFs reach 8,036 kN and 14,593 kN, respectively. Moreover, when the PIF is 30,000 kN, the punching shear failure also happen at the impact area on the reference column (C0) [6]. From Eq. 21, the value of k_T in these three cases are 6.56, 6.7, and 6.12, respectively. Based on these results, in this study, k_T is suggested as 6.5. Hence, the dynamic shear capacity of the RCBC, which is also the largest peak impact force that could be generated from a vehicle impact, is:

$$P_{dyn}^{\max} = 6.5 \times \frac{f_c}{10} \times D \times W \tag{22}$$

where f_c is the compressive strength of concrete.

The maximum dynamic shear capacity of the column is defined based on the contribution of concrete, reinforcements, and inertia in two sides of the shear plug, as shown in Figure 14b. However, the diagonal shear crack on the two sides will not happen at the same time because of the boundary condition effects. The lower side of the shear plug is close to the footing and it is affected by the boundary condition while the top side of the shear plug does not connect to the boundary. For a RC column under vehicle collision, to form a punching shear failure on the column, a diagonal shear crack firstly occurs at the column base due to the influence of the boundary condition and then another diagonal shear crack occurs on the other side of the impact point on the column, as illustrated in Fig. 14a. This phenomenon is observed consistently in the numerical simulations and can be physically explained based on the effect of the inertial resistance and the boundary effect. Therefore, when the PIF from collision events is larger than the dynamic shear capacity of the column, it will cause a diagonal shear failure. Because the shear resistance along the column is identical, the dynamic shear capacity of one side of the shear plug is $0.5P_{dyn}^{\max}$. Based on the proposed equation, it can be concluded that when the PIF from a collision event is higher than $0.5P_{dyn}^{\max}$, the diagonal shear failure at the impact area will occur in the RC column at the column base. If the PIF is equal to $P_{dyn}^{\max}$, punching shear failure occurs. The comparison of the proposed equation with the numerical and experimental results are given in Table 3. Moreover, the numerical results also illustrate the significant contribution of the column properties, i.e. column dimension and concrete strength in determining the impact force profile from vehicle collisions. When the PIF on the column is larger than a half of the maximum dynamic shear capacity of the column, which depends on the column cross-section dimension and the tensile strength of concrete, either diagonal shear or punching shear failure occurs in the column, the second PIF from the cargo impact will not happen, leading to the change of the impact force profile.

6. Column responses and failure classification

Fig. 16 shows the maximum bending moment and shear force in the RCBCs with different cross-section dimensions and column heights generated by vehicle impact. It should be noted that those curves are plotted by connecting the maximum value of the bending moment and shear force at multiple sections along the column. Those values at different sections occur at a different time instant, but all occur during the impact of the vehicle engine. The variation of the bending moment and shear force was presented and explained in the previous study [6]. The envelop curves are considered in this study while the time difference between the occurrence of these maximum values is not considered because the maximum values are the primary concerns in column design rather than the time instant when they occur. As can be seen from the figure, the bending moment and shear force diagram of the column can be divided into two separate groups, i.e. flexural response in which the negative bending moment occurs at the base and the column top while the positive bending moment happens at the impact point and the intermediate section, e.g. Fig. 16a - Load 1 (V = 100 km/h, m_e = 0.64 ton) and shear response where the bending moment at the intermediate section occurs in the negative side of the column, e.g. Fig. 16a - Load 2 (V = 100 km/h, m_e = 2.0 ton) and Load 3 (V = 120 km/h, m_e = 2.0 ton). As shown in Fig. 16a, under Load 1, similar maximum bending moment curves are achieved in the Columns C0, C4, and C6-8 where the flexural response is observed in these columns with no diagonal shear or punching shear failure. When the RCBCs are impacted by Load 2, the diagonal shear crack forms in the Columns C0 and C4 while the punching shear occurs in the column C6 (see Table 3) resulting in a significant change in the maximum bending moment curve. These three columns thus suffer shear failure with the maximum bending moment at the intermediate section shifting from the positive side to the negative side of the column. The bending moment shape of the columns C7 and C8 in Load 2 is almost unchanged compared to that under the first loading condition and no shear crack occurs at the column base after the PIF. The PIF increases to about 26,000 kN under Load 3, the Column C7 suffers a diagonal shear crack at the base which leads to the change of the bending moment curve from the flexural response to shear response (see Fig. 16a – Load 3). Besides, the bending moment shape of the Columns C0, C4, and C6 is similar to that under the previous loading condition but the intermediate section suffering flexural damage moves downward towards the impact point while the bending moment shape of the Column C8 is similar to that under the first two loading conditions. The maximum shear force of those columns under the three loading conditions are also plotted in Fig. 16b. It is very clear from the figure that when the column is under flexural response, the shear force at the base reaches the maximum value on the negative side while the shear force at the top occurs on the positive side (see Fig. 16b - Load 1). However, when the shear cracks occur at the column base, the maximum shear force at the column top moves to the negative side (Column C0, C4, and C6 in Load 2-3; C7 in Load 3). The change of the bending moment and shear force when a shear crack occurs in the column at the base can be explained by the formation of a shear plastic hinge at the impact area, as shown in Fig. 17. When impact does not induce shear failure in the vicinity of the collision point, with the large inertia resistance from superstructures and the short duration of the engine impact, the column responses to the impact force follow a column with fixed boundary conditions at the two ends (see Fig. 17a) even though the rigidity of the two ends is different, implying the large mass on top of the column provides a large inertial resistance, making the top of the column similar to having a fixed boundary condition during the impact of the engine. However, when impact induces shear cracks in the column, i.e. diagonal shear and punching shear which form a shear plastic hinge at the impact point, the column reacts to the impact force as a fixed-fixed column with the hinge at the impact point, the bending moment and shear force distribution of the column change (see Fig. 17b). Moreover, it is worth mentioning that although the PIF applied on the above columns is similar when these columns are under the same loading condition, the column with larger cross-section shows a larger maximum bending moment and shear force at critical sections (see Fig. 16 – Load 2-3). This is because according to the dynamic equilibrium equation when two columns with different cross-sections are impacted with a similar impact force, the column with larger cross-section will provide a higher elastic resistance because of the larger column stiffness, which leads to larger bending moment and shear force in the column.

The crack patterns and failure of those columns impacted by the three impact loading conditions are also presented in Fig. 18. As can be seen that when punching shear failure (C6) happens in the RCBC, negative flexural cracks occur in the vicinity of the impact point (1 – 2 m) in both Load 2 and Load 3. A similar observation was reported in the previous study by Zhao et al. [33] in which the maximum bending in the negative side was formed at 1.5 m away from the impact point when the beam experienced the punching shear failure. For the Columns C0 and C4, the flexural response is observed when these columns are under the impact of Load 1. When a diagonal shear failure forms at the impact area, a flexural – shear crack happens in the negative side of the column in both Load 2 and Load 3 (see Figs. 18b and 18c). Furthermore, after yielding the diagonal shear crack at the base (see Fig. 18c), Column C7 exhibits another flexural – shear crack near the column top. No shear failure and flexural – shear crack in the negative side of the column is observed in the Column C8 in all of the loading conditions.

From the above observations and discussions, the column responses and failures are classified into two categories: flexural response and shear response as summarized in Fig. 19. The column shows a flexural response when the PIF from the vehicle impact is smaller than $0.5P_{dyn}^{\max}$ and no diagonal shear crack forms in the column. Under this condition, the intermediate section and flexural cracks occur on the positive side of the column. When the PIF is higher than $0.5P_{dyn}^{\max}$, a diagonal shear crack appears at the column base leading to the formation of flexural cracks on the negative side of the column. The increase of PIF in this range will lead to the downward trend of the intermediate section with flexural cracks. When the PIF reaches the maximum dynamic shear capacity of the column, $P_{dyn}^{\max}$, the punching shear failure occurs in the column with the intermediate section of flexural cracks being formed closer to the impact point and at 1.5 – 2 m above the impact point.

7. Conclusions

This study numerically investigates the impact behaviour of RCBCs under vehicle collision. A series of FE models of full-scale bridge columns under collision of a medium truck and a large trailer are built and simulated. The effects of column parameters on the impact force time histories and the column response under three different conditions have been examined. The findings of this study can be summarized as follows:

1. An analytical model is proposed to predict the vehicle impact loading profile on rectangular RC columns corresponding to four continuous stages, i.e. bumper impact, engine impact, truck rail impact, and cargo impact. The results indicate that the vehicle

impact force time histories depend on both the column parameters and initial conditions of the vehicle model. A good agreement between the proposed model and numerical simulations has been achieved.

2. Owing to the damage of the column to vehicle engine impact, the cargo impacts of all the considered numerical cases do not generate a peak impact force larger than that from engine impact, but could generate a larger impulse depending on the impact conditions and cargo mass. The results imply that in most common cases of bridge columns, the peak impact force is associated with the vehicle engine impact while the maximum impulse could be associated with either engine impact or cargo impact. Assuming a rigid column or neglecting column damage in numerical simulations likely overestimate the impact force, especially the cargo impact force.
3. The maximum dynamic shear capacity of the column has been defined in which the column cross-section dimension and concrete strength provide the most contribution to the shear capacity before cracking while the contribution of the steel reinforcement is significant only after concrete cracking.
4. Based on the maximum dynamic shear capacity of the column and the PIF from the collision, the column failure mode can be classified into two separate groups, i.e. flexural failure $\left(PIF < 0.5P_{dyn}^{\max}\right)$ and shear failure $\left(PIF \geq 0.5P_{dyn}^{\max}\right)$. In the design, the dynamic resistant capacity of column needs to be provided to resist the column global damage, i.e. flexural cracks at the base, impact area, intermediate section, and column top, as well as the local failures, i.e. diagonal shear failure and punching shear failure.

Acknowledgment

This study is supported by Australian Research Council (ARC) (DP 150104346). The first author would like to acknowledge the financial support from the Curtin International Postgraduate Research Scholarship (CIPRS) to undertake his Ph.D. study.

References

[1] Buth CE, Williams WF, Brackin MS, Lord D, Geedipally SR, Abu-Odeh AY. Analysis of large truck collisions with bridge piers: phase 1. Report of guidelines for designing bridge piers and abutments for vehicle collisions. *Rep FHWA/TX-10/9-4973-1*Texas Transportation Inst., College Station, TX; 2010.

[2] Chen L, Xiao Y. Review of studies on vehicle anti-collision on bridge piers. J Highway Transp Res Dev. 2012;29:78-86.

[3] Buth CE, Brackin MS, Williams WF, Fry GT. Collision loads on bridge piers: phase 2. Report of guidelines for designing bridge piers and abutments for vehicle collisions. *Rep FHWA/TX-11/9-4973-2,* Texas Transportation Inst., College Station, TX; 2011.

[4] Sharma H, Hurlebaus S, Gardoni P. Performance-based response evaluation of reinforced concrete columns subject to vehicle impact. Int J Impact Eng. 2012;43:52-62.

[5] Abdelkarim OI, ElGawady MA. Performance of bridge piers under vehicle collision. Eng Struct. 2017;140:337-52.

[6] Do TV, Pham TM, Hao H. Dynamic responses and failure modes of bridge columns under vehicle collision. Eng Struct. 2018;156:243-59.

[7] Agrawal AK. Bridge vehicle impact assessment.New York State Department of Transportation, University Transportation Research Center; 2011.

[8] Agrawal AK, Liu GY, Alampalli S. Effects of truck impacts on bridge piers. Advanced Materials Research: Trans Tech Publ; 2013. p. 13-25.

[9] Chen L, El-Tawil S, Xiao Y. Reduced models for simulating collisions between trucks and bridge piers. J Bridge Eng. 2016;21:04016020.

[10] Al-Thairy H, Wang Y. An assessment of the current Eurocode 1 design methods for building structure steel columns under vehicle impact. J Constr Steel Res. 2013;88:164-71.

[11] AASHTO. AASHTO LRFD bridge design specifications (customary U.S. units). 6th Ed., Washington, DC2012.

[12] SA/SNZ. Structural design actions Part 1: Permanent, imposed and other actions Sydney, NSW 2001; Wellington 6020: AS/NZS 1170.1:2002; 2002.

[13] CEN. Actions on structures. Part 1-1: General actions-densities, self-weight, imposed loads for building. European Committee for Standardization. Brussels, Belgium: BS EN 1991-1-1:2002; 2002.

[14] CEN. Actions on structures. Part 1-7: General actions-accidental actions European Committee for Standardization. Brussels, Belgium: BS EN 1991-1-1:2002; 2006.

[15] El-Tawil S, Severino E, Fonseca P. Vehicle collision with bridge piers. J Bridge Eng. 2005;10:345-53.

[16] Do TV, Pham TM, Hao H. Performances of Reinforced Concrete Bridge Columns under Vehicle Impact. 5th International Conference on Protective Structures. Poznan, Poland2018.

[17] Hu B, Li G-Q. Maximum Impact Force of Truck Frontal Crashing into Antiram Bollard Systems. J Struct Eng. 2016;142:04016125.

[18] Zhang X, Hao H, Li C. Experimental investigation of the response of precast segmental columns subjected to impact loading. Int J Impact Eng. 2016;95:105-24.

[19] LS-DYNA L. Keyword user's manual. Livermore Software Technology Corporation. 2007.
[20] Pham TM, Hao H. Influence of global stiffness and equivalent model on prediction of impact response of RC beams. Int J Impact Eng. 2018;113:88-97.
[21] Pham TM, Hao Y, Hao H. Sensitivity of impact behaviour of RC beams to contact stiffness. Int J Impact Eng. 2018;112:155-64.
[22] Li J, Hao H. Numerical study of concrete spall damage to blast loads. Int J Impact Eng. 2014;68:41-55.
[23] Li J, Hao H, Wu C. Numerical study of precast segmental column under blast loads. Eng Struct. 2017;134:125-37.
[24] Hao Y, Hao H. Influence of the concrete DIF model on the numerical predictions of RC wall responses to blast loadings. Eng Struct. 2014;73:24-38.
[25] Malvar LJ, Crawford JE. Dynamic increase factors for steel reinforcing bars [C]. 28th DDESB Seminar Orlando, USA1998.
[26] Abdelkarim OI, ElGawady MA. Performance of hollow-core FRP–concrete–steel bridge columns subjected to vehicle collision. Eng Struct. 2016;123:517-31.
[27] Consolazio G, Davidson M. Simplified dynamic analysis of barge collision for bridge design. Transportation Research Record: Journal of the Transportation Research Board. 2008:13-25.
[28] Megally SH, Garg M, Seible F, Dowell RK. Seismic performance of precast segmental bridge superstructures. SSRP. 2001:24.
[29] Bakis CE, Ganjehlou A, Kachlakev DI, Schupack M, Balaguru P, Gee DJ et al. Guide for the design and construction of externally bonded FRP systems for strengthening concrete structures. Reported by ACI Committee. 2002;440.
[30] Chen L, Xiao Y, Xiao G, Liu C, Agrawal AK. Test and numerical simulation of truck collision with anti-ram bollards. Int J Impact Eng. 2015;75:30-9.
[31] Do TV, Pham TM, Hao H. Impact Response and Capacity of Precast Concrete Segmental versus Monolithic Bridge Columns. J Bridge Eng. 2019.
[32] Do TV, Pham TM, Hao H. Numerical investigation of the behavior of precast concrete segmental columns subjected to vehicle collision. Eng Struct. 2018;156:375-93.
[33] Zhao D-B, Yi W-J, Kunnath SK. Shear Mechanisms in Reinforced Concrete Beams under Impact Loading. J Struct Eng. 2017;143:04017089.
[34] Pham TM, Hao H. Effect of the plastic hinge and boundary conditions on the impact behavior of reinforced concrete beams. Int J Impact Eng. 2017;102:74-85.
[35] Chen L, El-Tawil S, Xiao Y. Response spectrum-based method for calculating the reaction force of piers subjected to truck collisions. Eng Struct. 2017;150:852-63.
[36] Yi W-J, Zhao D-B, Kunnath SK. Simplified approach for assessing shear resistance of reinforced concrete beams under impact loads. ACI Struct J. 2016;113:747.
[37] Saatci S. Behaviour and modelling of reinforced concrete structures subjected to impact loads.Ph.D, University of Toronto; 2007.
[38] Pham TM, Hao H. Impact behavior of FRP-strengthened RC beams without stirrups. J Compos Constr. 2016;20:04016011.
[39] Adhikary SD, Li B, Fujikake K. Strength and behavior in shear of reinforced concrete deep beams under dynamic loading conditions. Nuclear Engineering and Design. 2013;259:14-28.

List of figures

List of tables

Tables

Table 1. Numerical results of vehicle impacts on the RCBC (medium truck)

No	Parameter		Dimensions (mm)			Load 1			Load 2			Load 3		
			W (mm)	*D* (mm)	*H* (mm)	P_1 (kN)	F_1 (kN)	P_2 (kN)	P_1 (kN)	F_1 (kN)	P_2 (kN)	P_1 (kN)	F_1 (kN)	P_2 (kN)
C0	Reference		1,200	1,200	9,600	1,636	8,261	1,408	1,673	18,247	1,129	1,952	24,174	1,356
C1	Slenderness	4	1,200	1,200	4,800	1,637	8,214	1,505	1,694	17,706	1,119	1,976	24,182	1,433
C2		5	1,200	1,200	6,000	1,668	7,504	1,355	1,736	18,520	1,041	1,933	23,549	1,300
C3		6	1,200	1,200	7,500	1,632	7,852	1,365	1,691	18,222	1,202	1,899	23,515	1,426
C4		10	1,200	1,200	12,000	1,642	7,591	1,389	1,701	18,130	1,155	1,962	24,425	1,354
C5	Cross section dimensions		600	600	6,000	1,023	7,321	1,064	1,062	8,036	1,233	1,259	8,876	1,108
C6			800	800	6,400	1,387	8,037	1,342	1,436	14,956	1,043	1,603	14,593	1,086
C7			1,500	1,500	12,000	1,855	8,079	1,347	1,882	19,522	1,254	2,228	25,708	1,586
C8			2,000	2,000	16,000	2,191	8,544	1,360	2,256	20,611	1,181	2,527	26,589	1,241
C9	Transverse reinforcements	d8a200	1,200	1,200	9,600	1,603	7,839	1,174	1,746	18,766	1,133	1,961	23,491	1,601
C10		d14a100	1,200	1,200	9,600	1,645	8,310	1,214	1,697	18,645	1,200	1,972	23,795	1,647
C11	Longitudinal reinforcements	24d22	1,200	1,200	9,600	1,647	8,008	1,382	1,730	18,777	1,255	1,937	22,050	1,366
C12		24d36	1,200	1,200	9,600	1,649	8,290	1,343	1,795	17,966	1,121	1,919	21,830	1,469
C14	Initial axial load	20%	1,200	1,200	9,600	1,645	8,725	1,334	1,762	18,240	1,117	1,959	23,478	1,474
C15		40%	1,200	1,200	9,600	1,636	8,502	1,297	1,682	18,866	1,109	1,960	22,766	1,490
C16		60%	1,200	1,200	9,600	1,638	8,385	1,289	1,795	18,075	1,028	1,954	23,415	1,517

Table 2. Numerical results of vehicle impacts on the RCBC (heavy truck trailer)

	Vehicle model			First phase		Second phase		Third phase		Fourth phase	
No	m (ton)	m_e (ton)	V (km/h)	t_{P1} (ms)	P_1 (kN)	T_{F1} (ms)	$F1$ (kN)	t_{P2} (ms)	P_2 (kN)	t_{F2} (ms)	F_2 (kN)
H1	17	1.5	80	46.5	1,623	11.5	11,904	40.0	750	38.0	6,000
H2	17	1.5	100	35.0	1,834	9.5	17,648	34.0	985	39.5	6,250
H3	17	1.5	110	31.0	1,848	8.0	19,025	30.5	960	34.0	6,610
H4	30	1.5	80	46.5	1,682	11.5	12,252	39.5	808	50.0	7,071
H5	37	1.5	80	46.5	1,651	11.5	11,867	39.5	768	60.0	6,926

Table. 3. Comparison between the proposed equation and available results

Reference	No	ID	Structural properties W (mm)	Structural properties D (mm)	Structural properties f_c (Mpa)	Numerical result (kN)	Experimental result (kN)	Failure	Proposed equation (kN)	Error (%)
This study	1	C5	600	600	34.0	8,036	--	Punching shear	7,956	10.4
	2	C6	800	800	34.0	14,593	--	Punching shear	14,144	3.1
Do et al. [6]	4	C14	1,200	1200	34.0	30,000	--	Punching shear	31,824	6.1
Pham et al. [21]	5	Beam 1	150	250	46.0	1,000	--	Punching shear cracks	1,121	12.0
	6	Beam 2	150	250	52.0	1,420	1,390	Punching shear cracks	1,268	8.7
Yi et al. [36]	7	BD4	150	310	41.4	1,470	1,465	Punching shear	1,242	15.2
Zhao et al. [33]	8	B-868-7.14	200	500	24.8	--	1,480	Punching shear	1,612	8.9
	9	C-868-7.14	200	500	26.3	--	1,735	Punching shear	1,709	1.5
	10	D-868-7.14	200	500	25.0	--	1,679	Punching shear	1,625	3.2
This study	11	C0	1,200	1,200	34.0	18,247	--	Diagonal shear failure	31,824	--
	12	C1	1,200	1,200	34.0	17,706	--	Diagonal shear failure	31,824	--
	13	C2	1,200	1,200	34.0	18,520	--	Diagonal shear failure	31,824	--
	14	C3	1,200	1,200	34.0	18,222	--	Diagonal shear failure	31,824	--
	15	C4	1,200	1,200	34.0	18,130	--	Diagonal shear failure	31,824	--
	16	C7	1,500	1,500	34.0	25,708	--	Diagonal shear failure	49,725	--

Note:--The value is not available or is not considered in this study

Figures

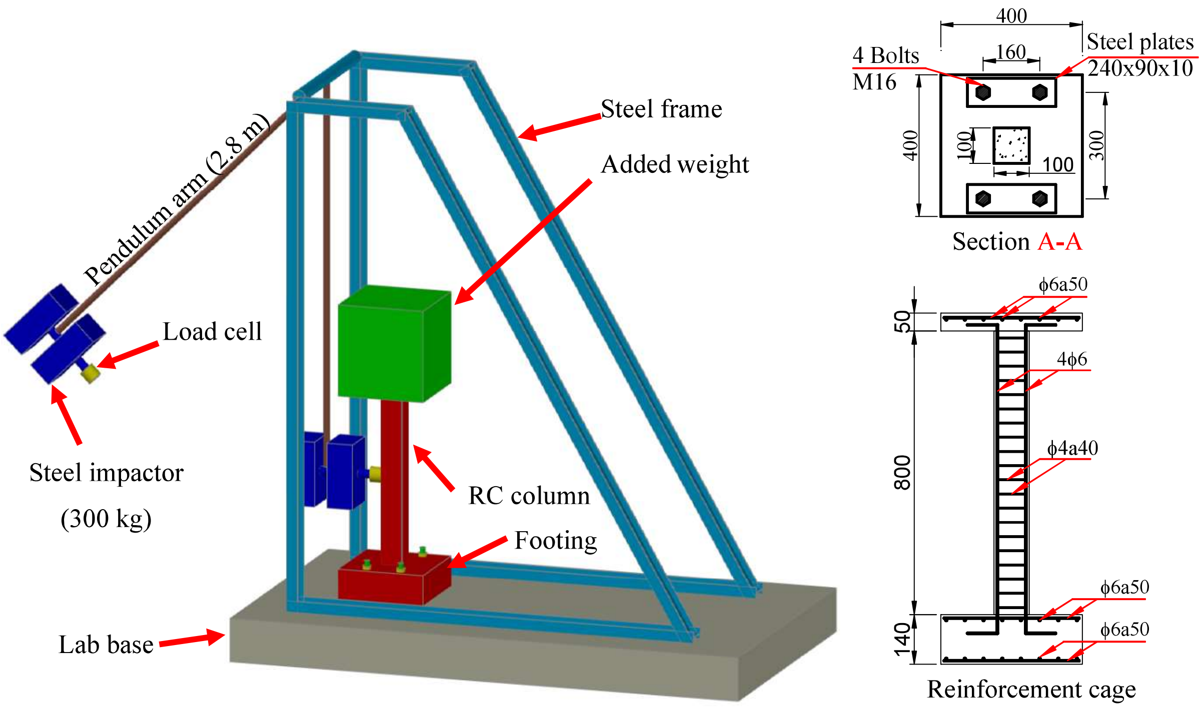

(a) Experimental test 3D view and the column design of the experimental test

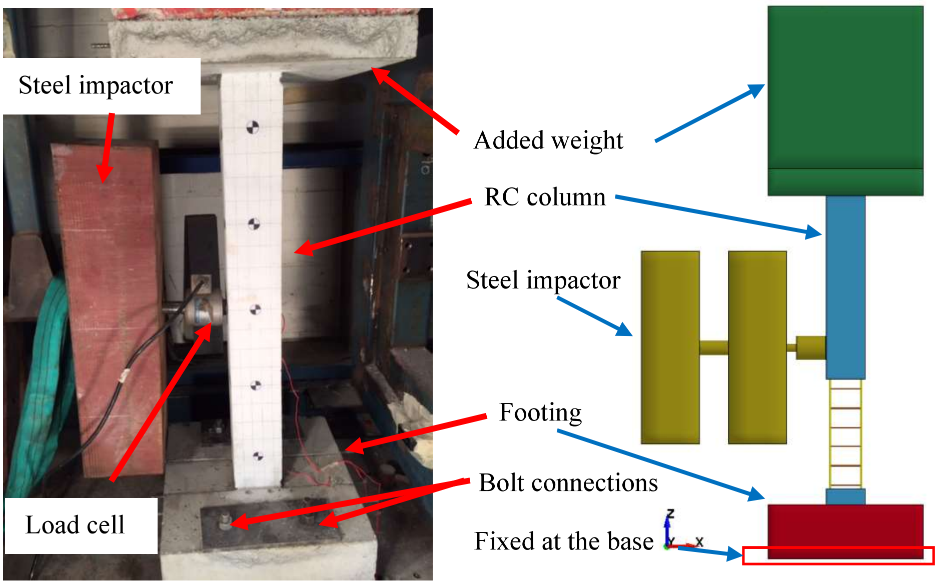

(b) Test set up and FE model of the RC column with the steel impactor

Fig. 1. Experimental test and FE model of the RC column under pendulum impact load

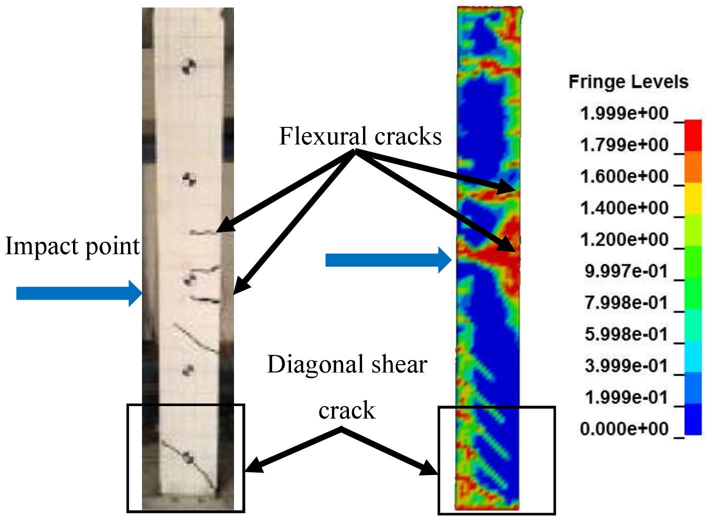

Experimental test Numerical simulation

(a) Plastic strain and column crack patterns

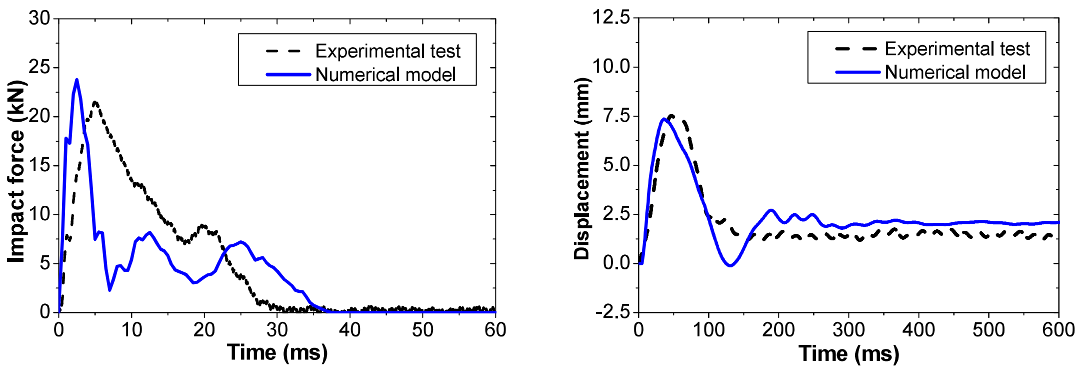

(b) Impact force time histories (c) Lateral displacement at the column mid-height

Fig. 2. Numerical model verification – the scale RC column under impact test

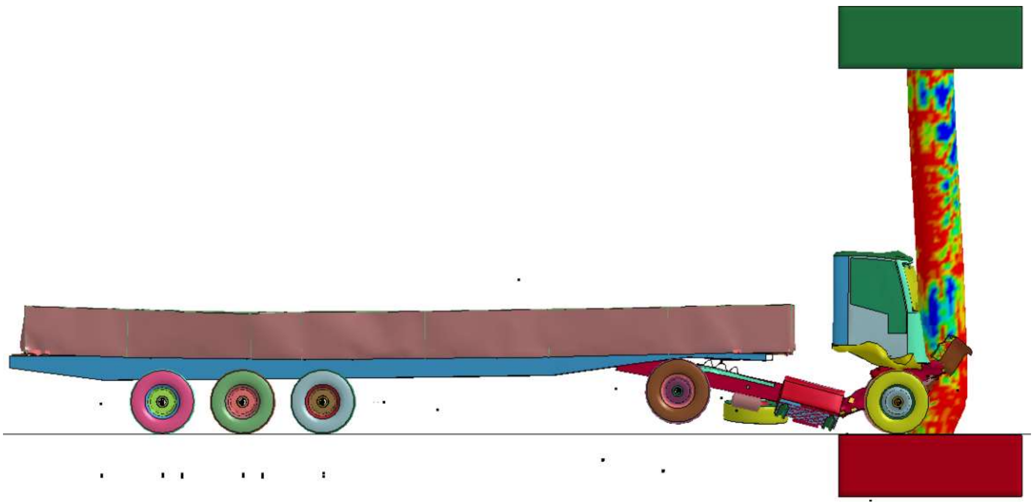

(a) Numerical model of the full-scale bridge column and heavy truck-trailer collision

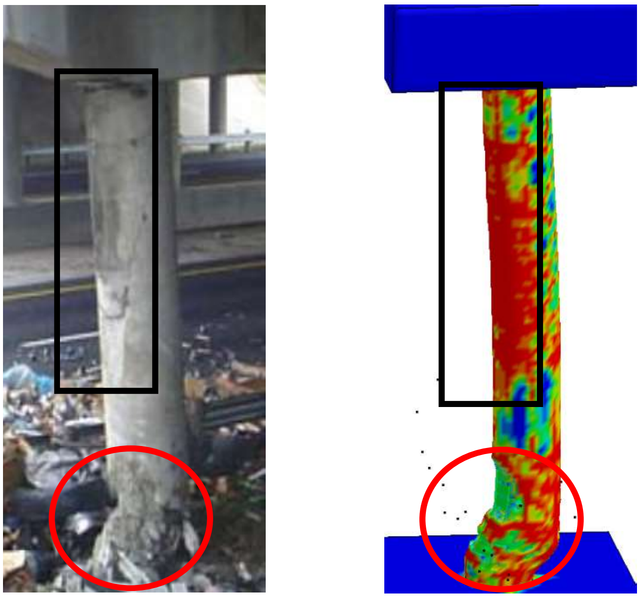

(b) Comparison of the column failure modes

Fig. 3. Numerical verification of the full-scale bridge model under heavy truck-trailer collision

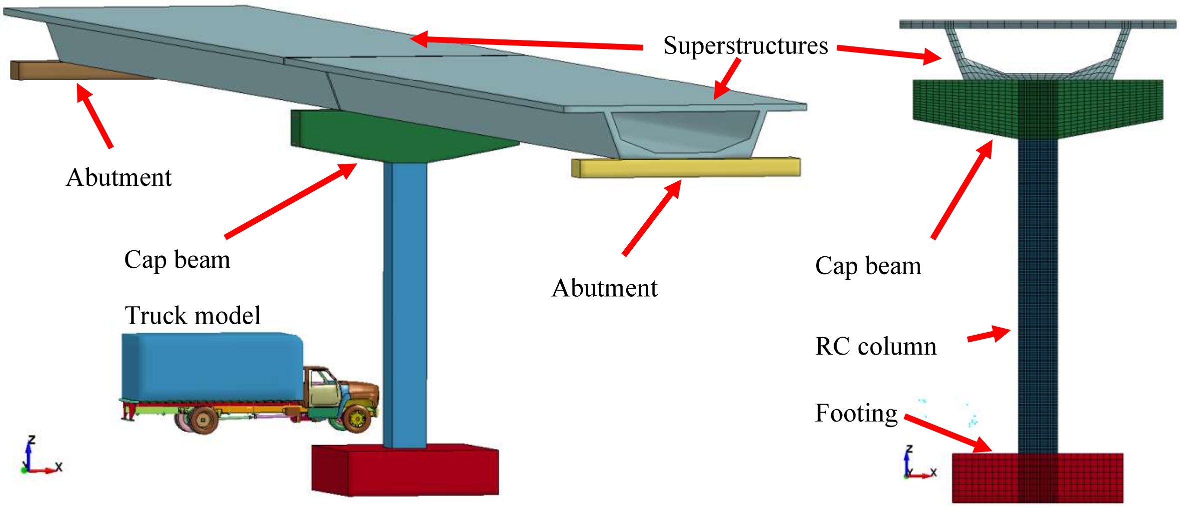

(a) 3D view (b) X-Z plane

Fig. 4. FE model of the RC bridge specimen

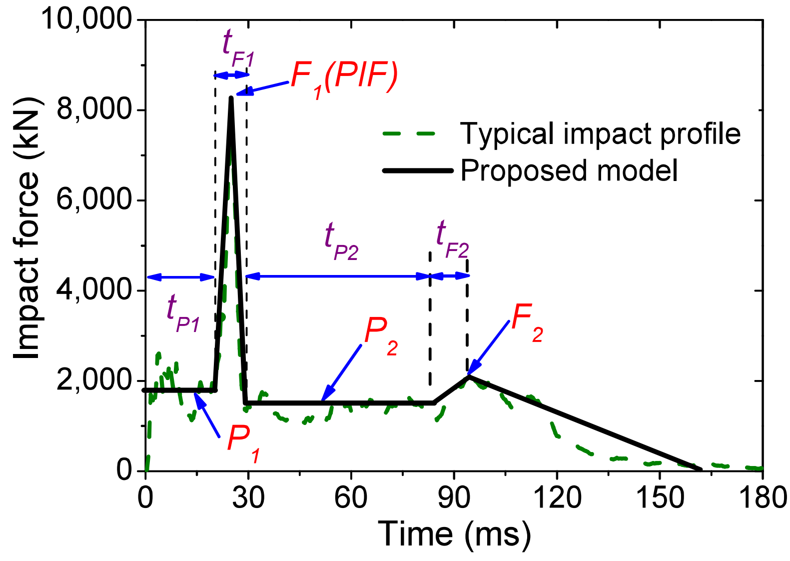

Fig. 5. A simplified model of the impact force time histories from the medium truck

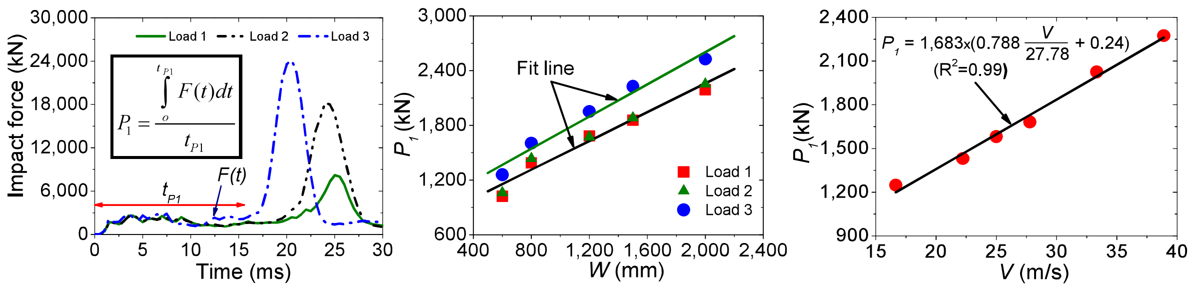

(a) (b) (c)

Fig. 6. The first phase of the impact force time histories: (a) Model of P1 and t_{P1}; (b) Column dimension versus P1 relationships; (c) Vehicle velocity versus P1 relationships

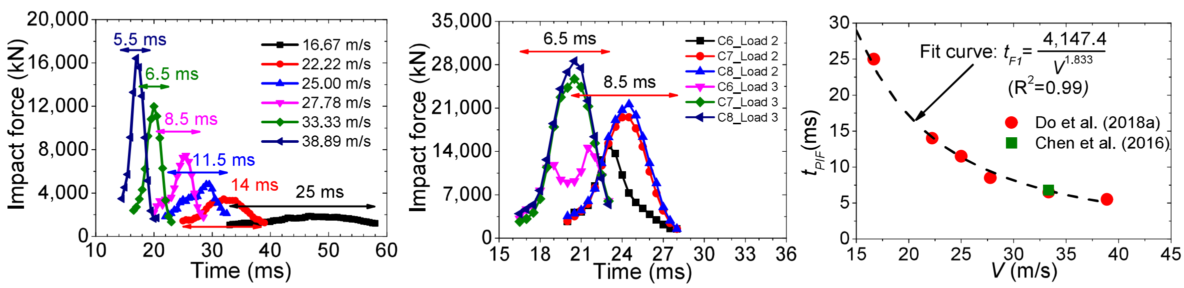

(a) (b) (c)

Fig. 7. The second phase of the impact force time histories: (a) The impact force corresponding to different vehicle velocities; (b) The impact force of different columns; (c) Vehicle velocity versus t_{F1} relationships

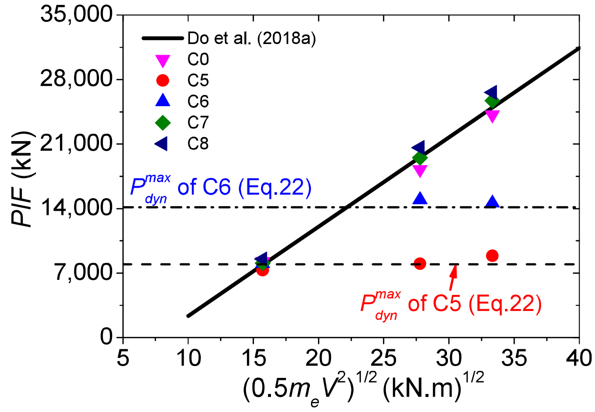

Fig. 8. The PIF of the RCBCs with different section dimensions under different loading conditions

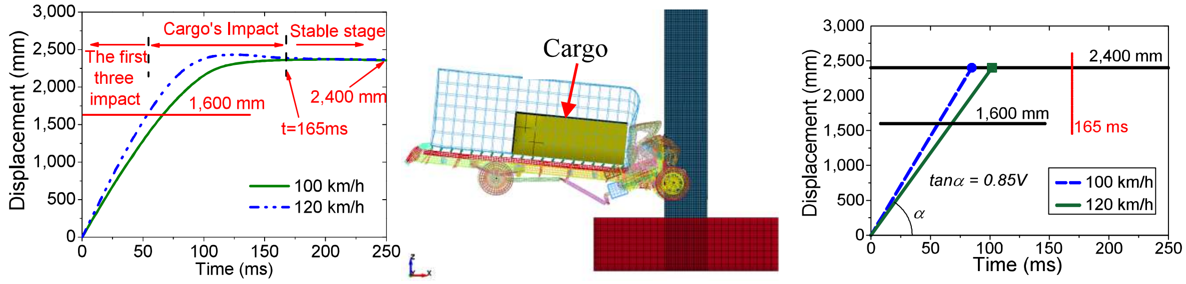

(a) (b) (c)

Fig. 9. The cargo's impact on the RCBC: (a) The cargo displacement time histories; (b) Vehicle deformation when the cargo collides on the column; (c) Simplified model of the cargo displacement

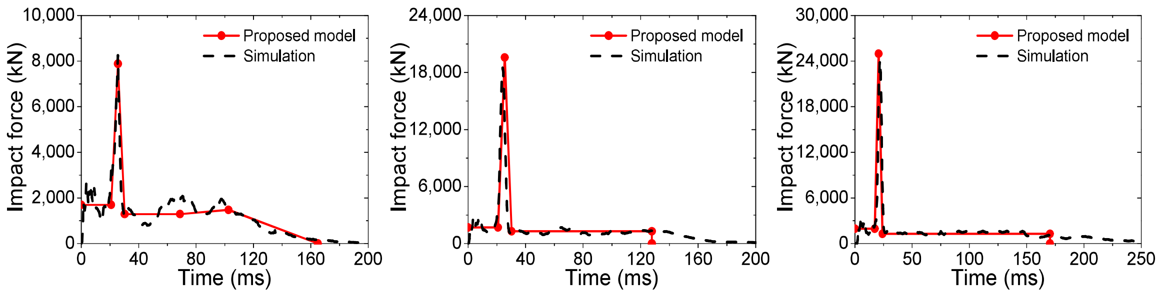

(a) Case C0 – Load 1 (b) Case C0 – Load 2 (c) Case C0 – Load 3

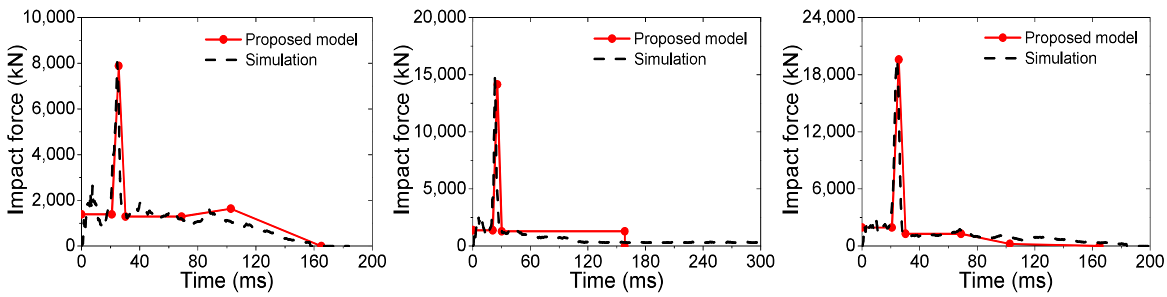

(d) Case C6 – Load 1 (e) Case C6 – Load 2 (f) Case C7 – Load 2

Fig. 10. The comparison between the proposed model and the numerical simulation (medium truck)

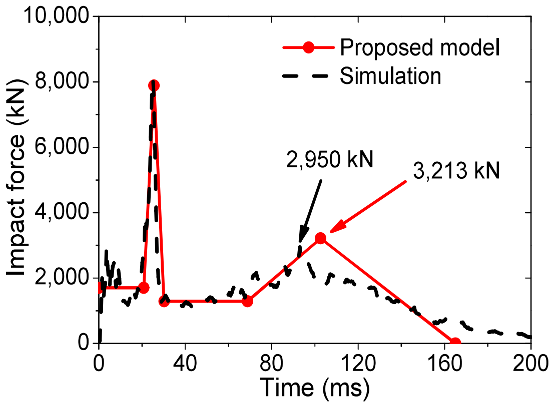

Fig. 11. Comparisons between the proposed model and numerical simulation with the vehicle mass of 11 ton (V = 100 km/h; m_e = 0.64 Ton, m = 11 ton)

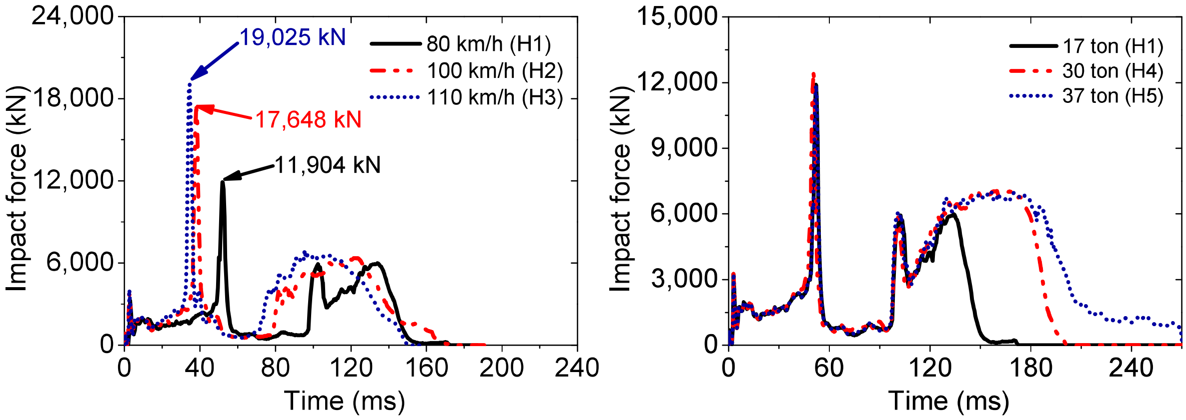

(a) Different vehicle velocities (b) Different vehicle mass

Fig. 12. Impact force time histories of the heavy truck model collided to the RCBC

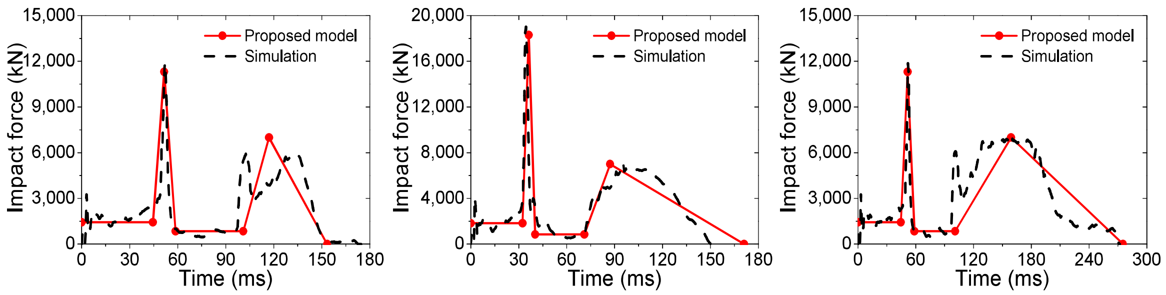

(a) H1 (b) H3 (c) H5

Fig. 13. The comparison between the proposed model and the numerical simulation (heavy truck trailer)

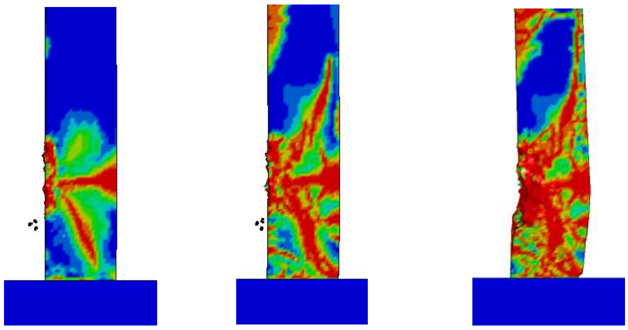

At PIF +2.0 ms post PIF Punching shear failure [6]

(a) Column punching shear failure

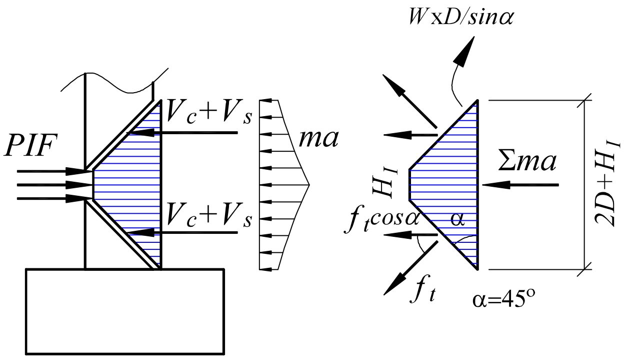

(b) Simplified punching shear model of the RCBC

Fig. 14. Shear mechanism of the RCBC under vehicle impact

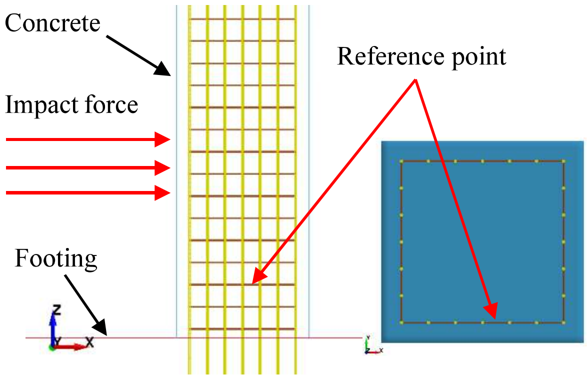

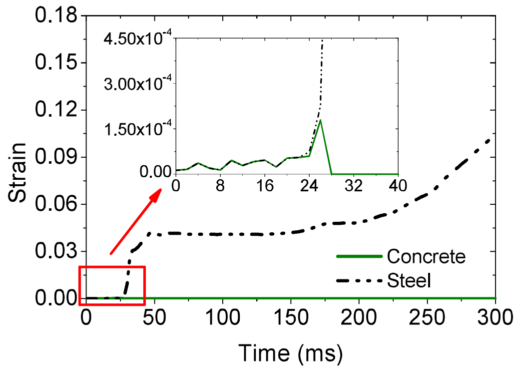

(a) (b)

Fig. 15. Strain of concrete and transverse steel under impact load: (a) Location of the reference point (b) Strain time histories of concrete and steel at the reference point (X direction)

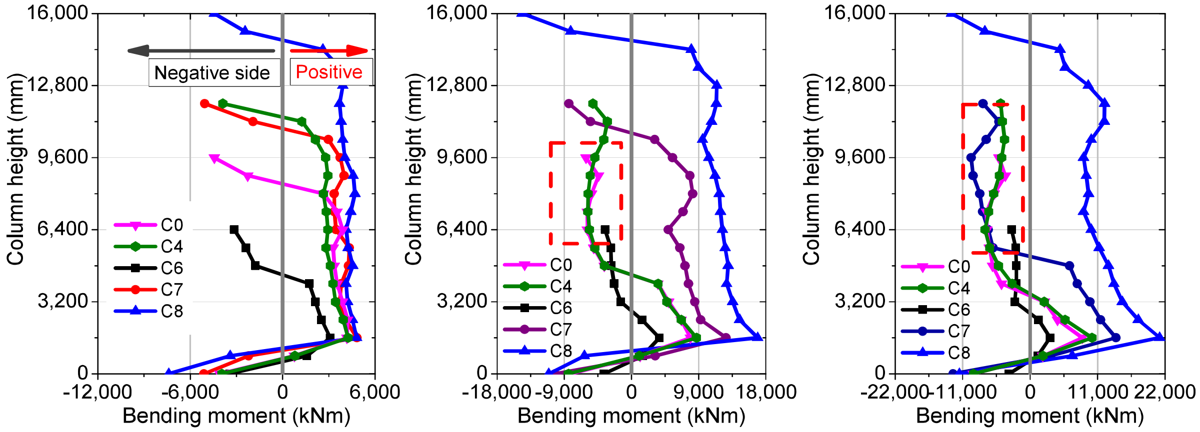

Load 1 Load 2 Load 3

(a) Maximum bending moment along the RCBC

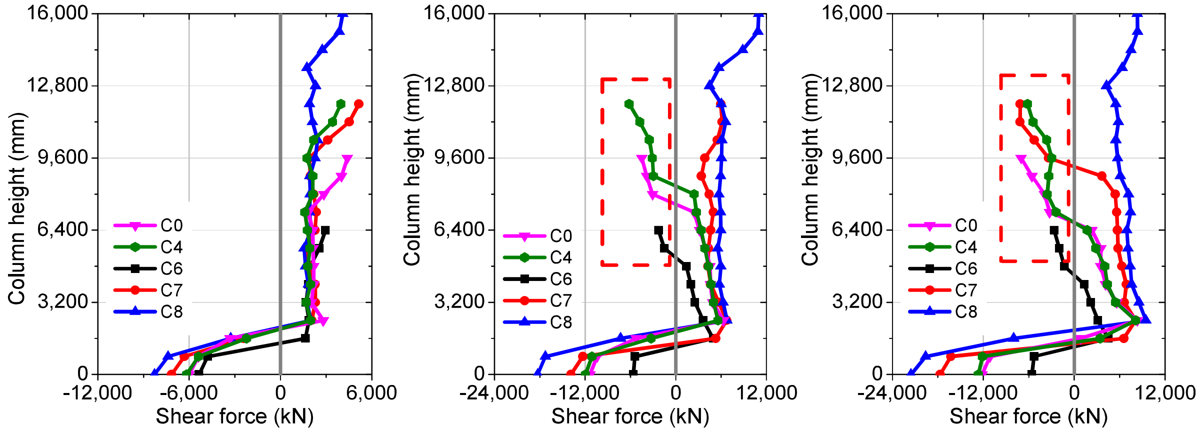

Load 1 Load 2 Load 3

(b) Maximum shear force along the RCBC

Fig. 16. Maximum bending moment and shear force of the RCBC under vehicle impact

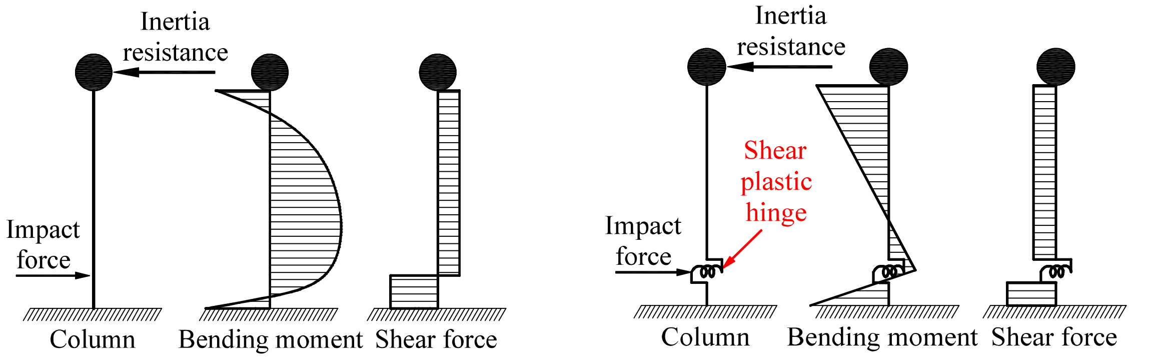

(a) No shear crack occurs (b) When diagonal shear or punching shear occurs

Fig. 17. Simple response of the column under PIF

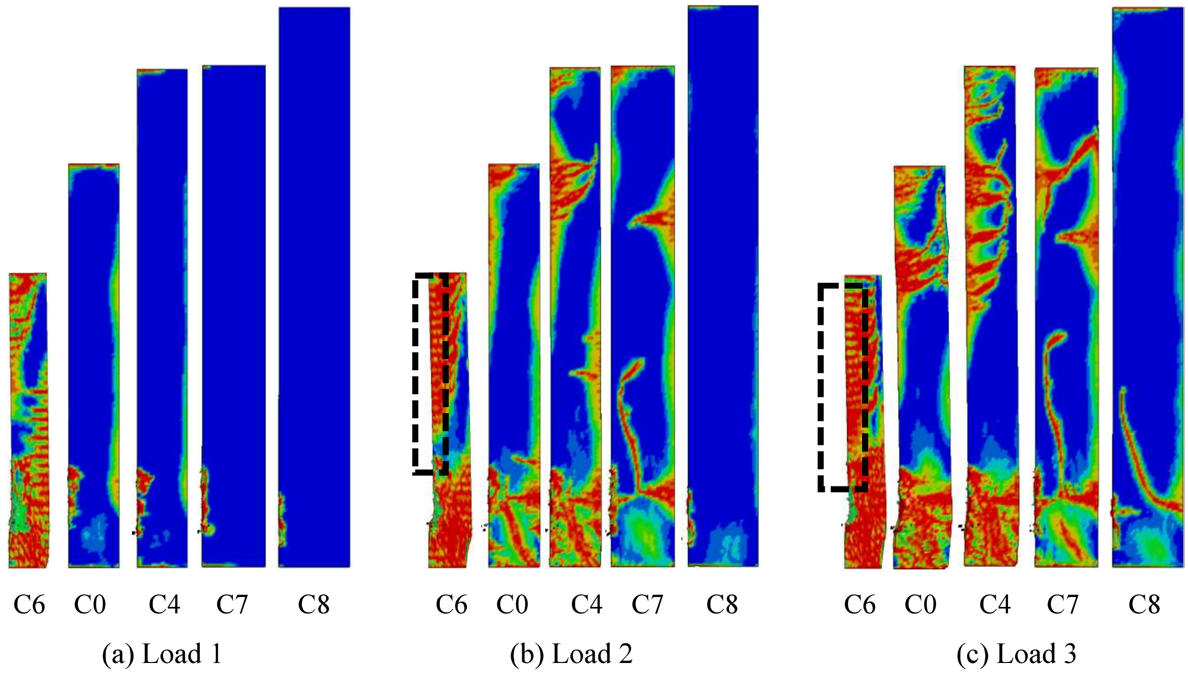

Fig. 18. Crack patterns and failure modes of the RCBC under vehicle impacts

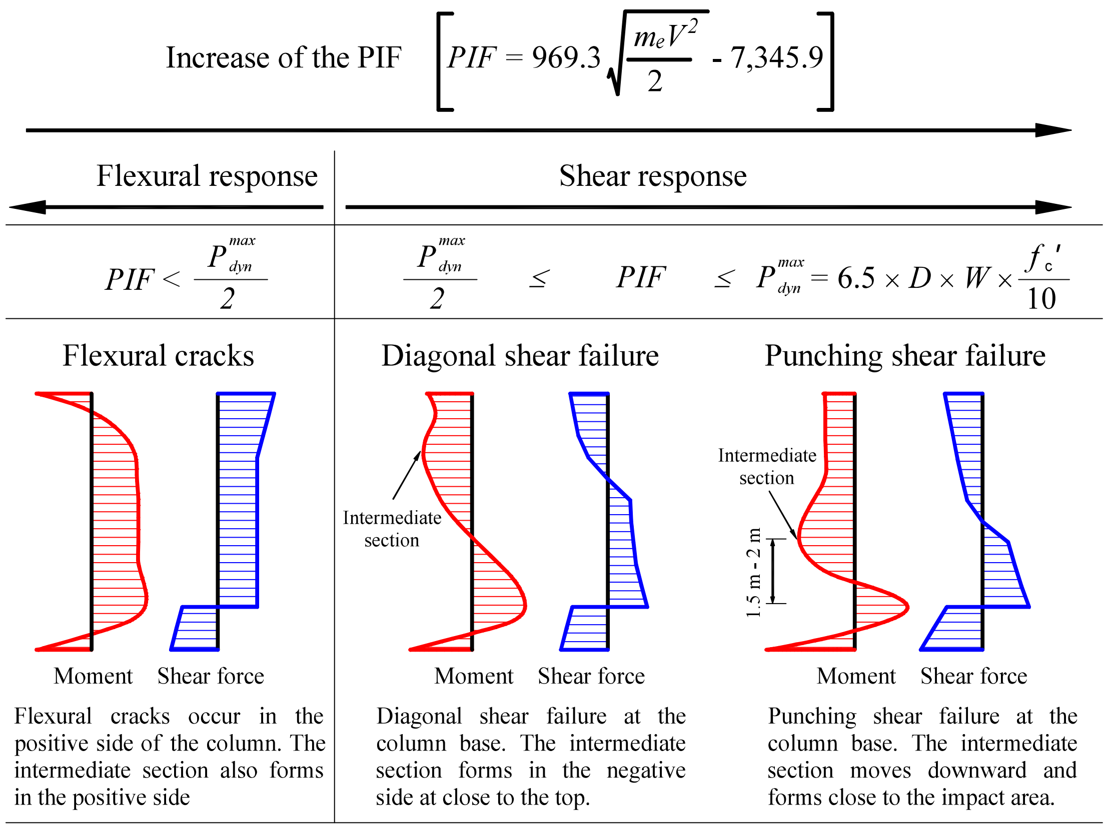

Fig. 19. Column response and failure classification under different PIF